ADVANCED MATERIALS

# Supporting Information

for *Adv. Mater.,* DOI: 10.1002/adma.201503567

## Arbitrary Shape Engineerable Spiral Micropseudocapacitors with Ultrahigh Energy and Power Densities

*Xiaocong Tian, Mengzhu Shi, Xu Xu, Mengyu Yan, Lin Xu, Aamir Minhas-Khan, Chunhua Han,* Liang He, and Liqiang Mai**

# Supporting Information

## Arbitrary Shape Engineerable Spiral Micropseudocapacitors with Ultrahigh Energy and Power Densities

*Xiaocong Tian, Mengzhu Shi, Xu Xu, Mengyu Yan, Lin Xu, Aamir Minhas-Khan, Chunhua Han,* Liang He, and Liqiang Mai**

**This file includes:**

Materials and devices characterization

Calculations of electrochemical performance

Figure S1. Dark-field microscopy optical and FESEM images of spiral-shaped SU-8 micro-pillar array.

Figure S2. Bright-field microscopy optical image after the secondary E-beam lithography alignments.

Figure S3. SEM images of the sample after platinum coating.

Figure S4. Schematic diagram showing the design of spiral-shaped MSCs.

Figure S5. XRD pattern of the electrodeposited active materials of cobalt hydroxide.

Figure S6. TEM images of the electrodeposited active materials of cobalt hydroxide.

Figure S7. FESEM images of SS-MPCs.

Figure S8. CV curves and capacitance of the bare platinum electrode.

Figure S9. Evolution of the stack energy and power densities of SST-MPCs.

Figure S10. Galvanostatic charge/discharge curve of SS-MPCs and SST-MPCs.

Figure S11. Nyquist plot and frequency response of SS-MPCs and SST-MPCs.

Figure S12. FESEM images of pillared three-dimensional micro-pseudocapacitors with the electrodeposited pre-intercalated manganese dioxides.

Figure S13. CV curves and capacitance of $MnO_2$-based micro-pseudocapacitors.

Figure S14. Comparison, in Ragone plots, of volumetric and areal specific energy and power densities of SST-MPCs and MSCs with laser-scribed graphene (LSG).

Figure S15. SEM image and CV curves of interdigital MPCs

Figure S16. The calculated electrical field distributions for circular and rectangular SST-MPCs.

## Materials and devices characterization

Materials characterization was conducted by FESEM (JEOL 7100F), optical microscopy, stylus surface profiler (Bruker DektakXT), and X-ray diffraction (Bruker D8 Discover X-ray diffractometer with non-monochromated Co-K$\alpha$ X-Ray source). CV, galvanostatic charge-discharge measurements and electrochemical impedance spectroscopy analysis examined at the scan rates of 0.01-200 V $s^{-1}$ were carried out based on the Autolab PGSTAT 302N. The loading amount of active materials is obtained through Atomic Absorption Spectroscopy (GBC Avanta).

## Calculations of electrochemical performance.

Based on the CV data, the capacitance values of MPCs were calculated according to the following equation (1): Ref.[1]

$$C_{\text{device}} = \frac{\int I(V)dV}{v * \Delta V} \tag{1}$$

Where $C_{\text{device}}$ represents the capacitance value of MPCs, $\Delta V$ is the scan range (in V), $\int I(V)dV$ is the integration in the charge-discharge process (in A·V), and $v$ is the scan rate (in V $s^{-1}$),.

Specific capacitances were calculated based on the area and stack volume of the device according to the following equation:

$$C_{\text{area}} = \frac{C_{\text{device}}}{A} \tag{2}$$

$$C_{\text{stack}} = \frac{C_{\text{device}}}{V} \tag{3}$$

Where $C_{\text{area}}$ (in F $cm^{-2}$) and $C_{\text{stack}}$ (in F $cm^{-3}$) refer to the area capacitance and stack stack capacitance of device, respectively. $A$ and $V$ are the total area ($cm^{-2}$) and volume ($cm^{-3}$) of the device, respectively. These capacitances were calculated by taking account the whole devices, including the electrodes and the interspaces between the electrodes.

Based on the galvanostatic charge-discharge measurement data, the capacitance values of MPCs were calculatedaccording to the following equation (4): Ref.[2]

$$C_{\text{device}} = \frac{I * \Delta t}{\Delta V * V} \tag{4}$$

Where $C_{\text{device}}$ represents the capacitance value of MPCs (in F $cm^{-3}$), $I$ corresponds to the discharge current (in A), $\Delta t$ is the discharge time (in s), $\Delta V$ is the voltage range excluding IR drop (in V) and $V$ is the volume (in $cm^{-3}$) of the device.

The energy density of the device was got according to the following equation (5):

$$E = \frac{C_{\text{stack}} * (\Delta V)^2}{7,200} \tag{5}$$

Where $E$ is the energy density (in Wh $cm^{-3}$), $C_{\text{stack}}$ is the stack stack capacitance (in F $cm^{-3}$), and $\Delta V$ is the potential range (in V).

The power density of the device was obtained from the following equation (6):

$$P = \frac{E}{\Delta t} * 3,600 \tag{6}$$

Where $P$ is the power density (in W $cm^{-3}$), $E$ is the energy density (in Wh $cm^{-3}$), $\Delta t$ is the discharge time (in s).

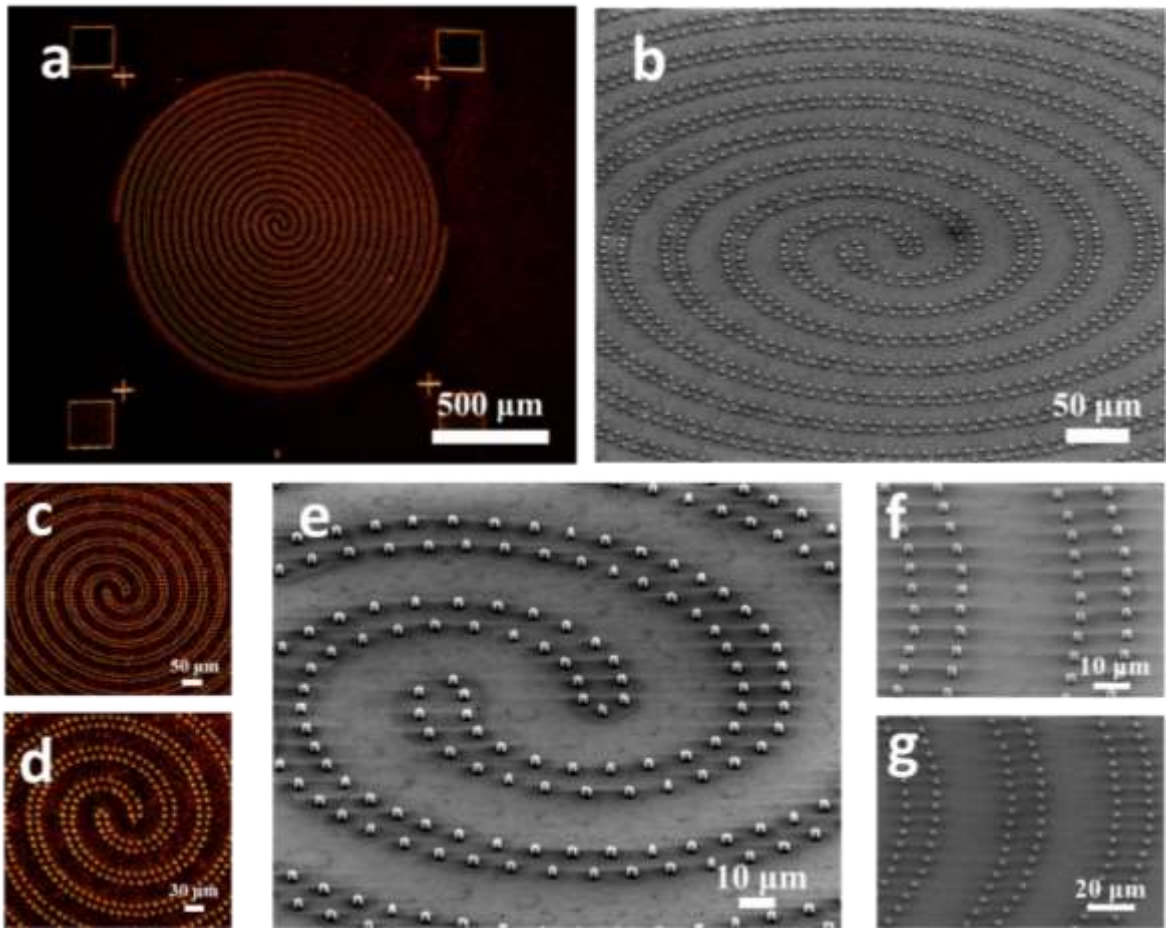


**Figure S1.** Dark-field microscopy optical a,c-d) and FESEM b,e-g) images of spiral-shaped SU-8 micro-pillar array.

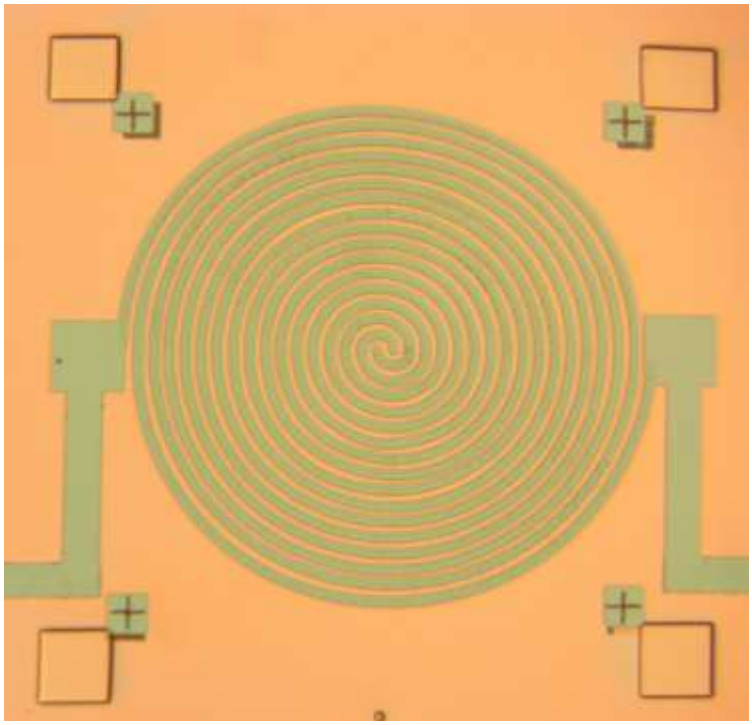

**Figure S2.** Bright-field microscopy optical image after the secondary E-beam lithography alignments.

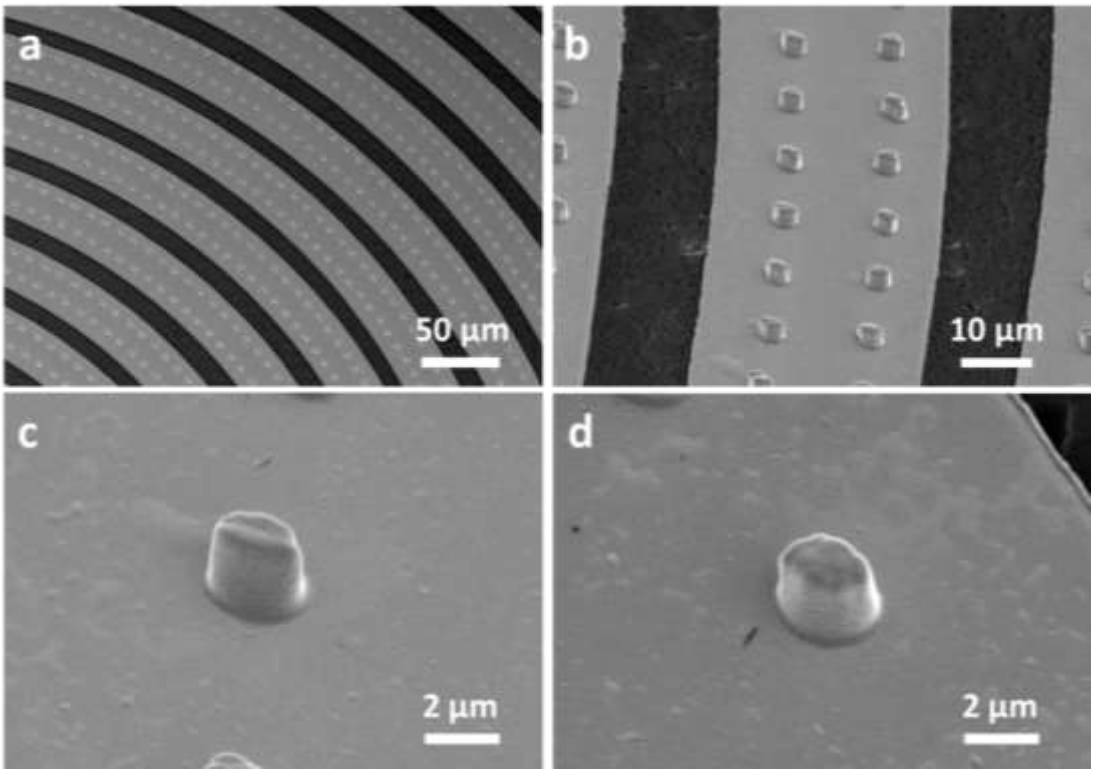


**Figure S3.** SEM images of the sample after platinum coating.

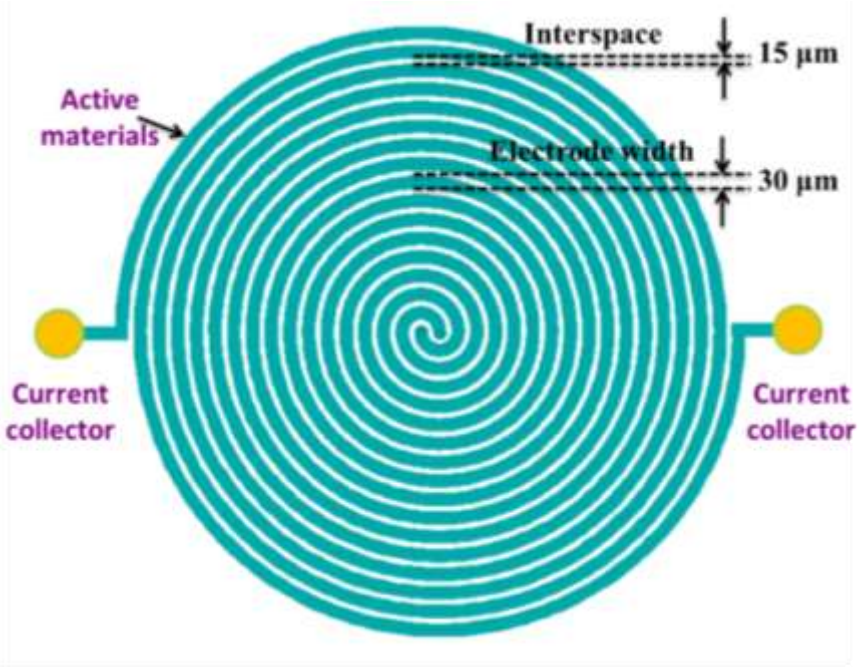


**Figure S4.** Schematic diagram showing the design of spiral-shaped MSCs. The total length of the one platinum electrode is approximately 18 mm.

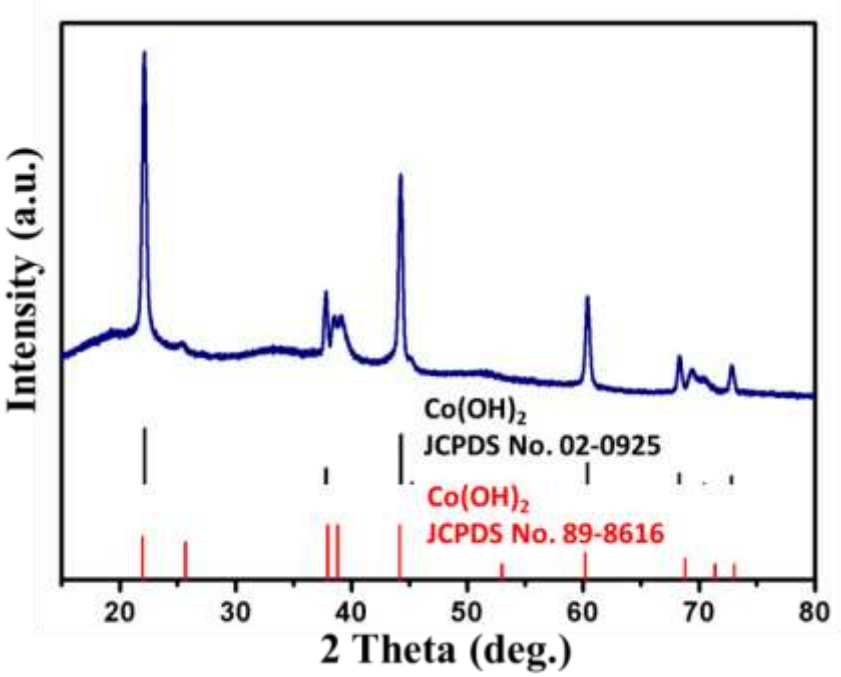


**Figure S5.** XRD pattern of the electrodeposited active materials of cobalt hydroxide.

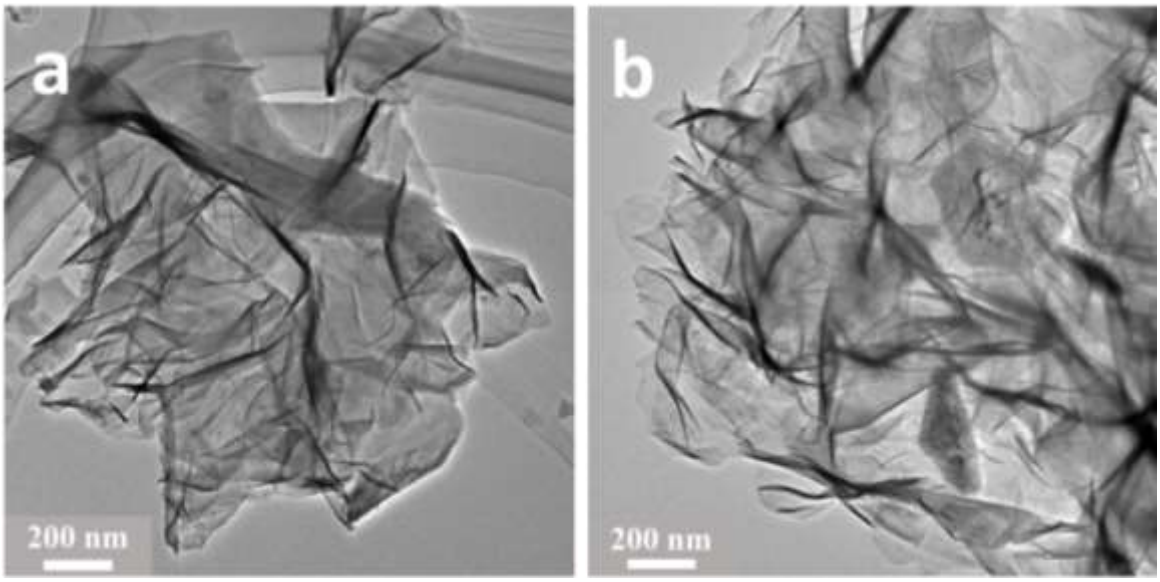


**Figure S6.** TEM images of the electrodeposited active materials of cobalt hydroxide.

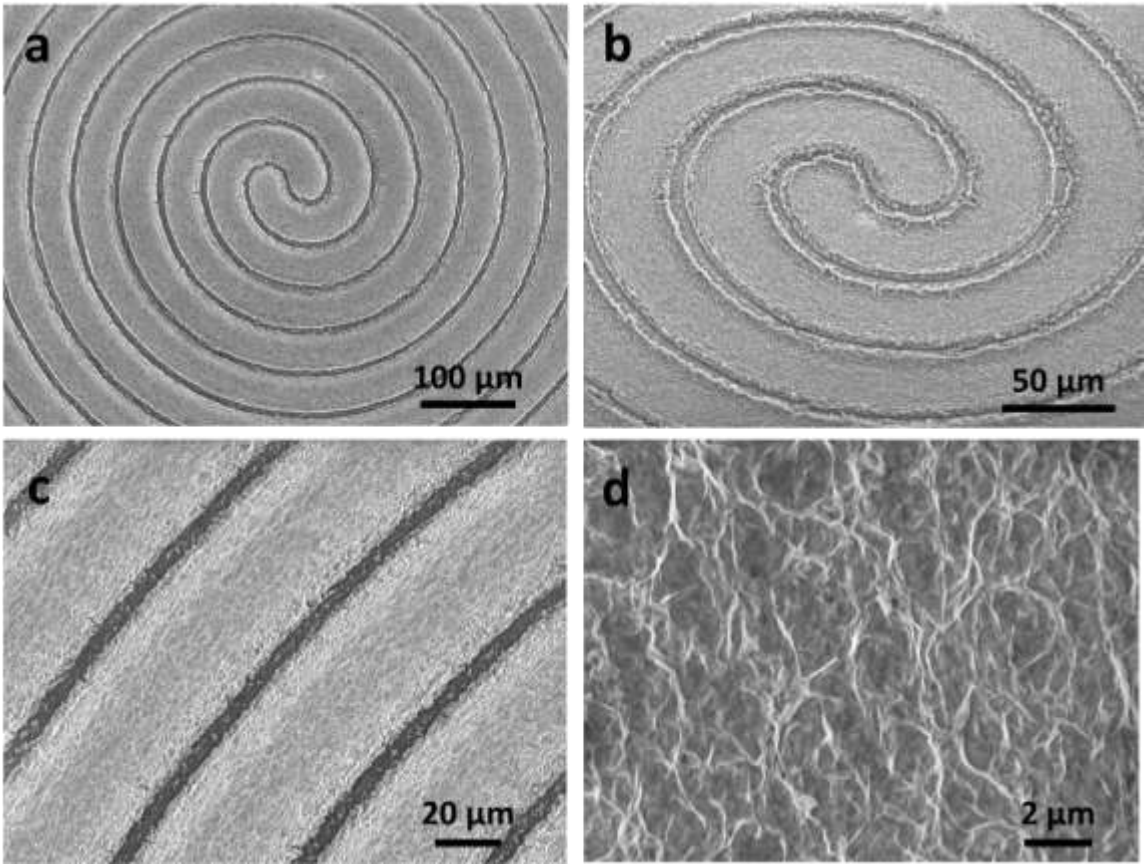


**Figure S7.** FESEM images of SS-MPCs.

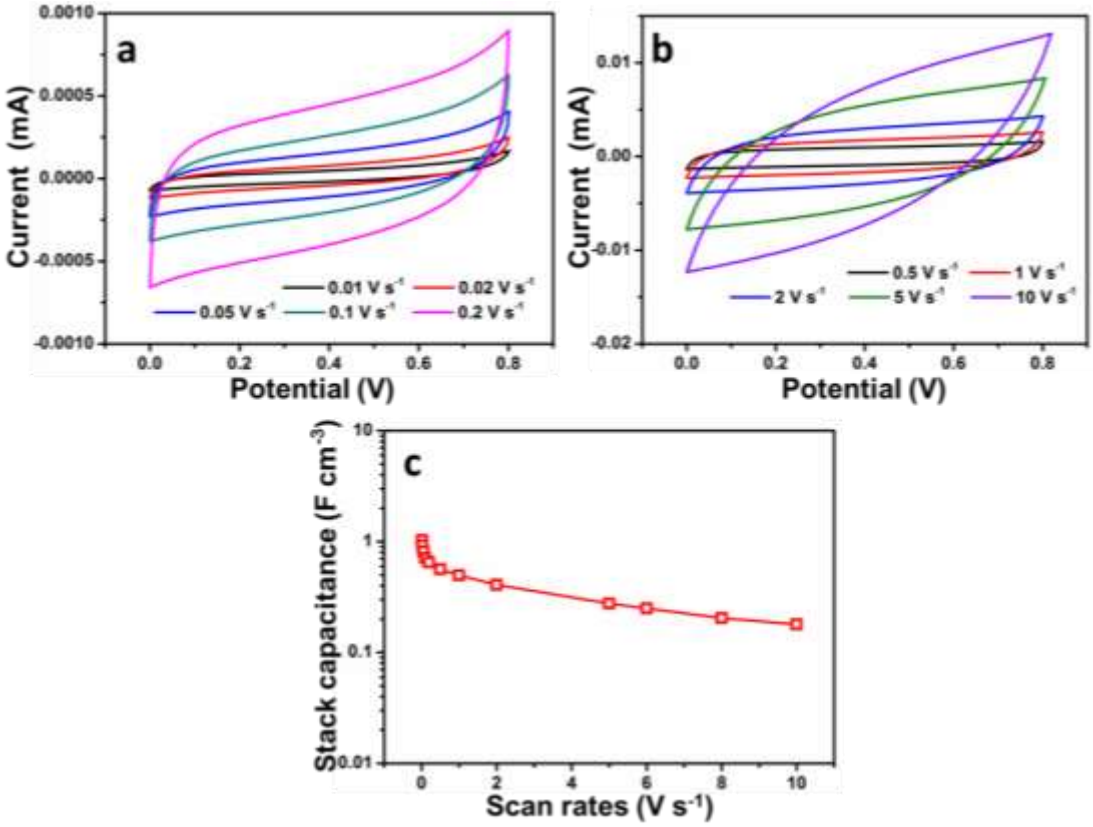


**Figure S8.** a,b) CV curves of the bare platinum electrode obtained at different scan rates. c) Evolution of the stack capacitance of the bare platinum electrode at different scan rates.

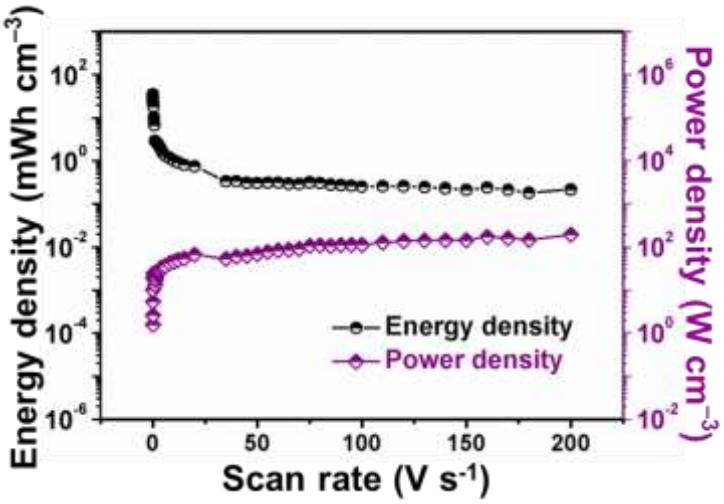


**Figure S9**. Evolution of the stack energy and power densities at different scan rates of SST-MPCs.

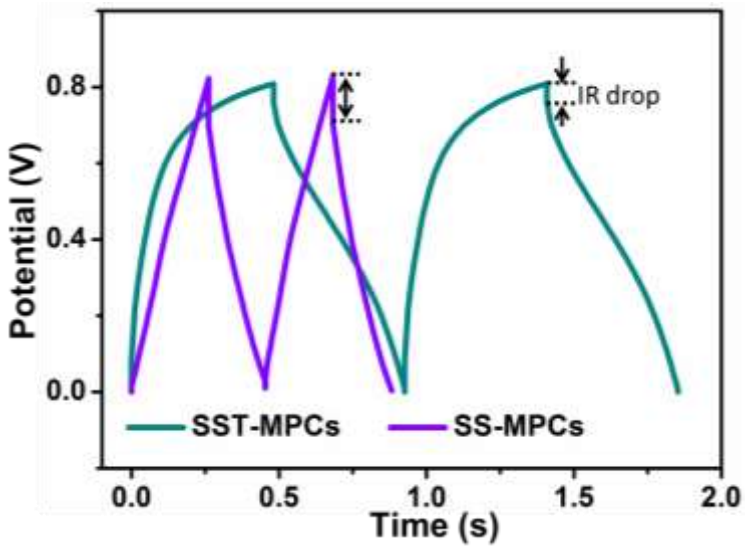


**Figure S10.** Galvanostatic charge/discharge curve of SS-MPCs and SST-MPCs at various current densitiy of 12.5 mA $cm^{-2}$.

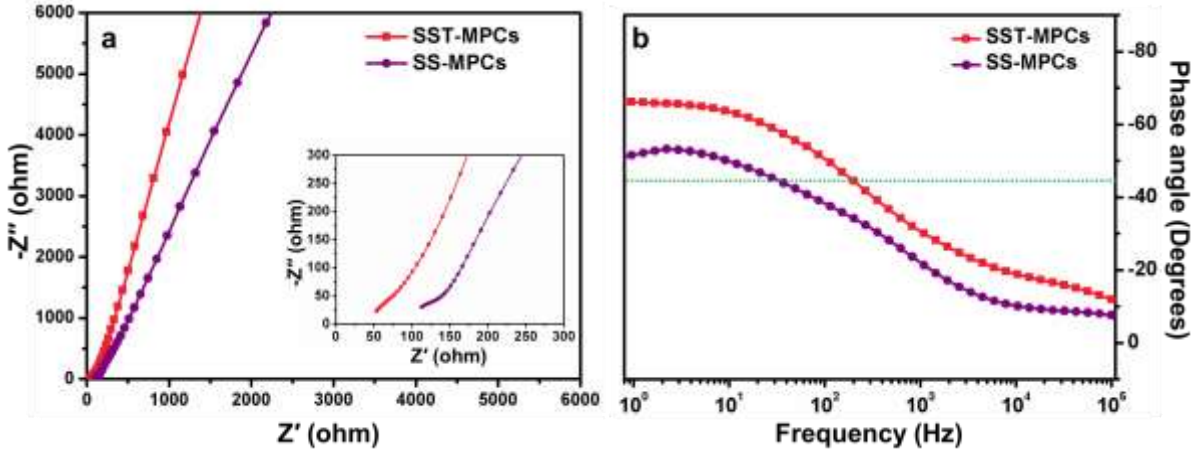


**Figure S11.** a) Nyquist plot of SS-MPCs and SST-MPCs from 0.5 Hz to 100 kHz. b) Impedance phase angle versus frequency for SS-MPCs and SST-MPCs.

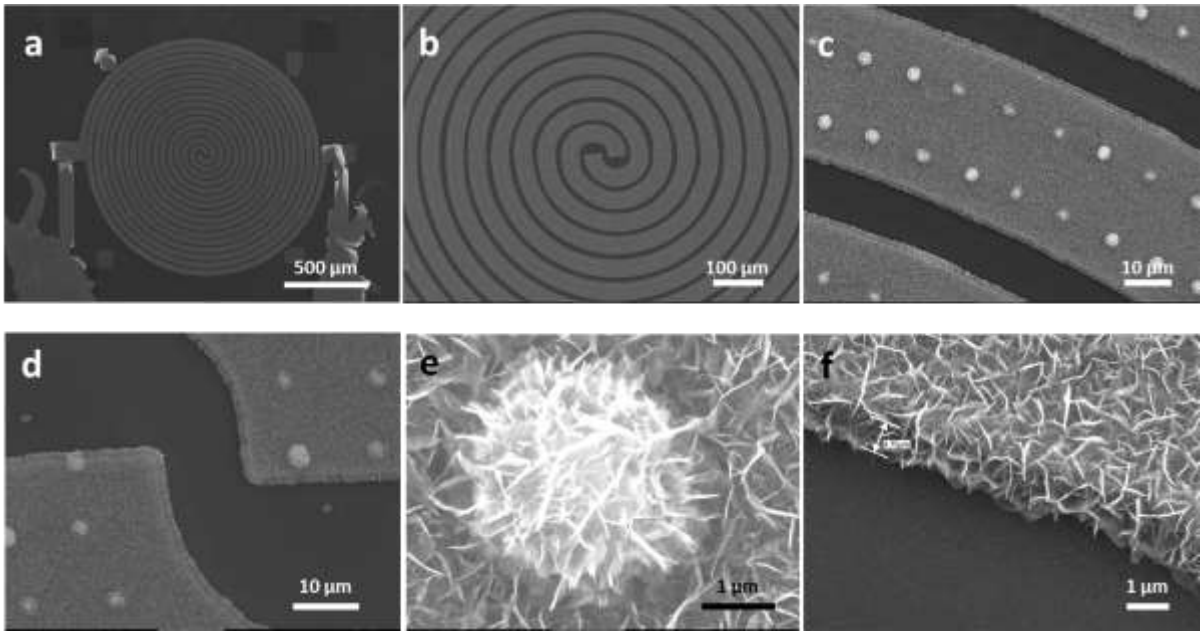


**Figure S12.** FESEM images of pillared three-dimensional micro-pseudocapacitors with the electrodeposited pre-intercalated manganese dioxides. The electrodeposition details are available in our previous paper.[3]

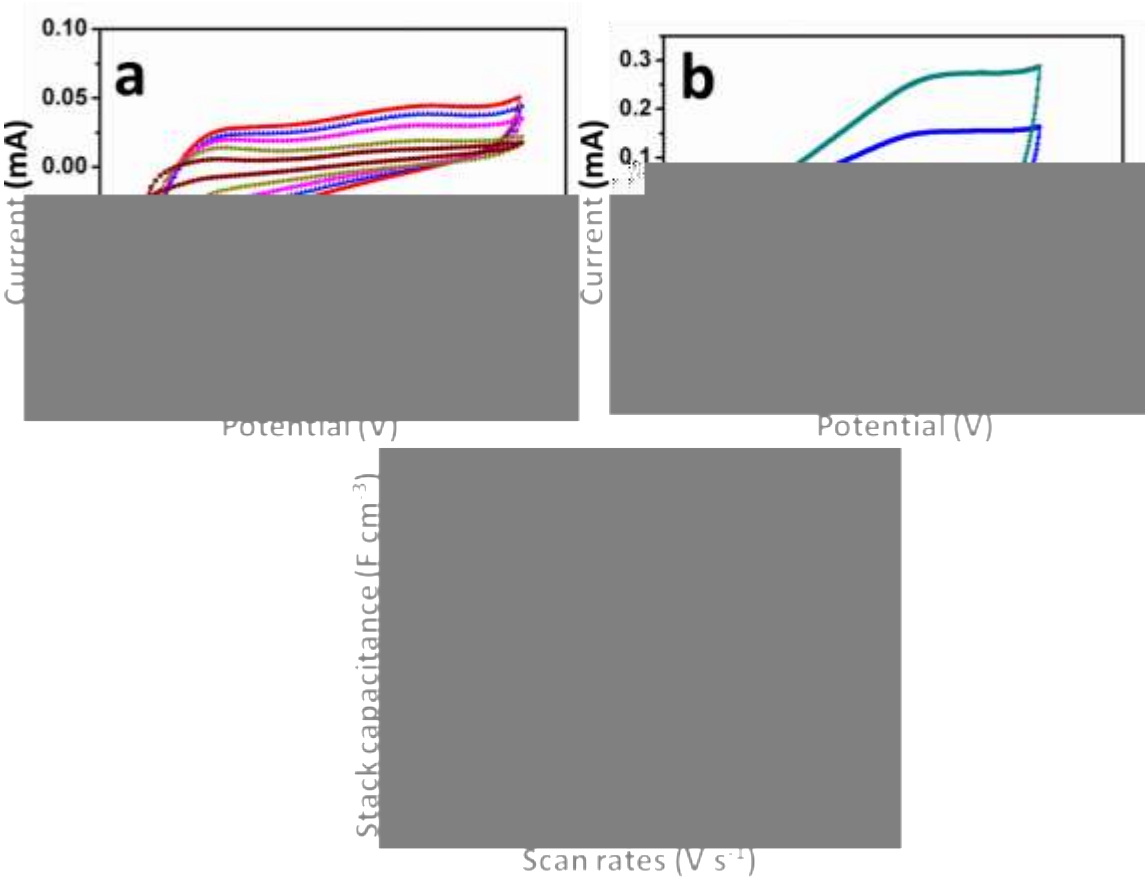


**Figure S13.** a,b) CV curves and b) evolution of the stack capacitance of $MnO_2$-based micro-pseudocapacitors obtained at different scan rates.

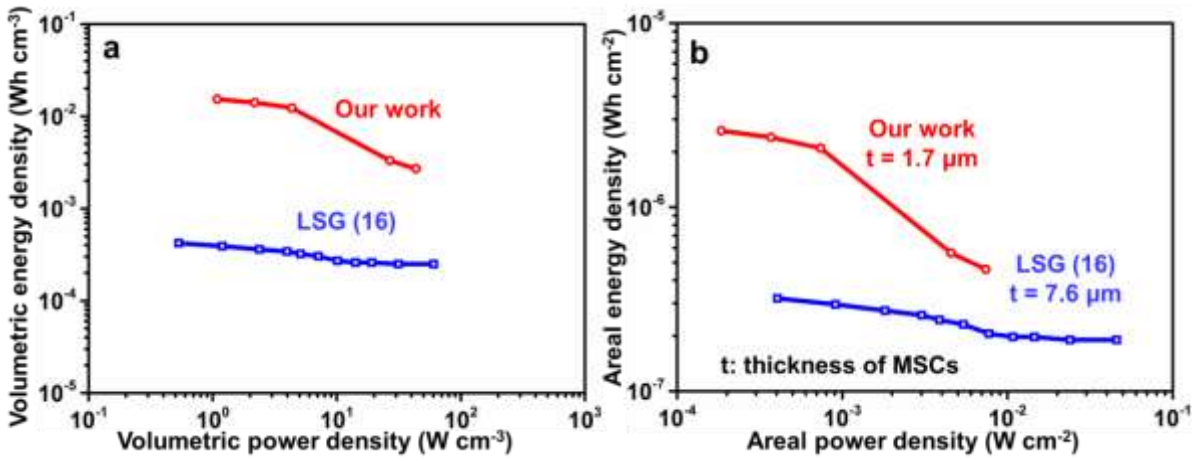


**Figure 14.** Comparison, in Ragone plots, of a) volumetric and b) areal specific energy and power densities of SST-MPCs and MSCs with laser-scribed graphene (LSG) based the galvanostatic charge-discharge method.

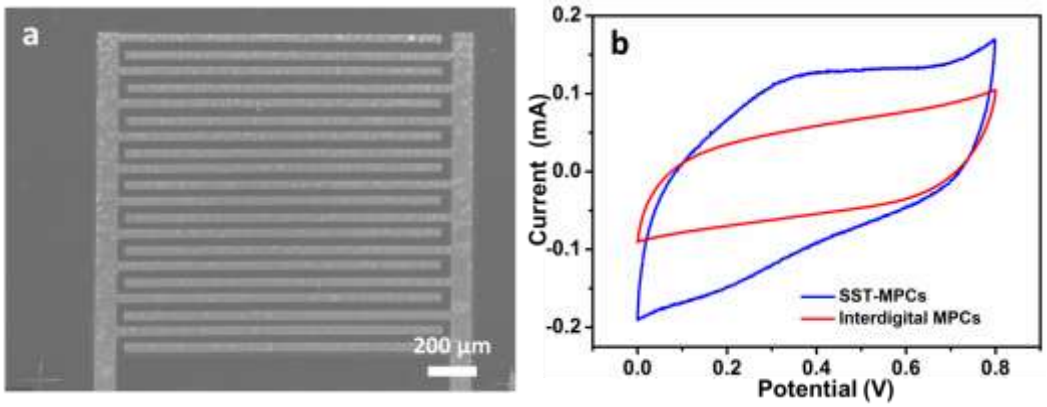


**Figure S15.** a) SEM image of interdigital MPCs. b) CV curves of interdigital MPCs and SST-MPCs at the scan rate of 2 V $s^{-1}$.

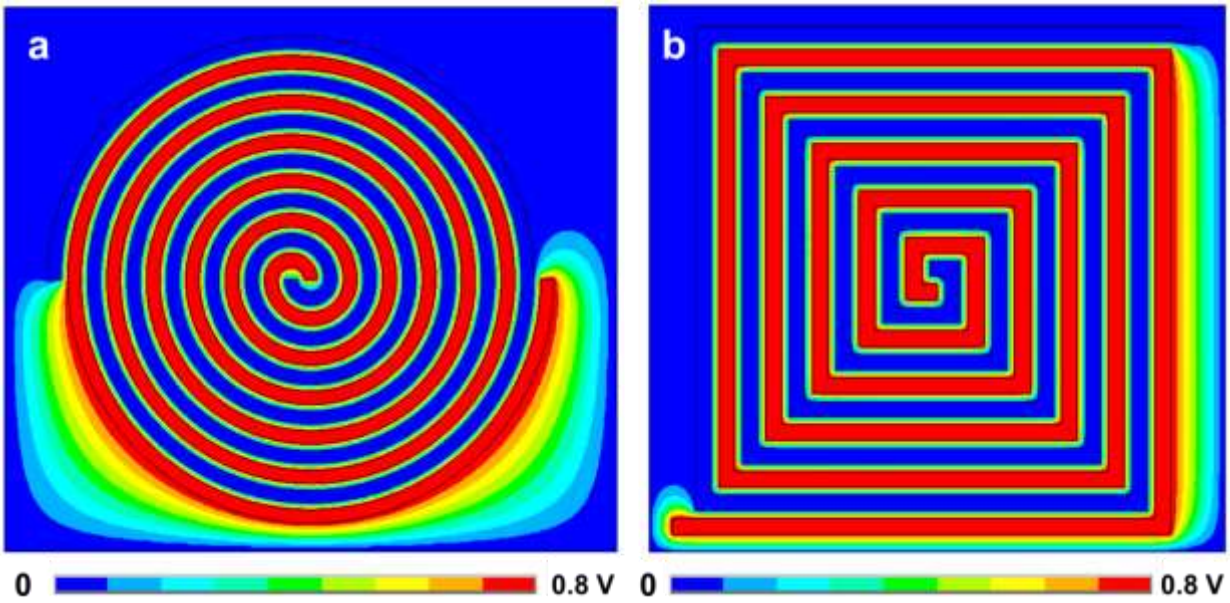


**Figure S16.** The calculated electrical field distributions for a) circular and b) rectangular SST-MPCs.

## Supplementary References.

[1] Z. S. Wu, K. Parvez, X. Feng, K. Müllen, *Nature Commun.* **2013**, *4*, 2487.

[2] G. Lee, D. Kim, D. Kim, S. Oh, J. Yun, J. Kim, S.-S. Lee, J. S. Ha, *Energy Environ. Sci.* **2015**, *8*, 1764.

[3] L. Mai, H. Li, Y. Zhao, L. Xu, X. Xu, Y. Luo, Z. Zhang, W. Ke, C. Niu, Q. Zhang, *Sci. Rep.* **2013**, *3*, 1718.